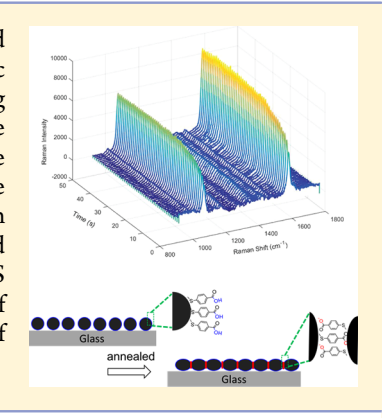
# In Situ Probing of Laser Annealing of Plasmonic Substrates with Surface-Enhanced Raman Spectroscopy

Chaoxiong Ma,<sup>†,§</sup> Kaiyu Fu,<sup>†,§</sup> Michael J. Trujillo,<sup>†</sup> Xin Gu,<sup>†</sup> Nameera Baig,<sup>†</sup> Paul W. Bohn,<sup>†,‡</sup> and Jon P. Camden<sup>\*,†</sup>

<sup>†</sup>Department of Chemistry and Biochemistry and <sup>‡</sup>Department of Chemical and Biomolecular Engineering, University of Notre Dame, Notre Dame, Indiana 46556, United States

Supporting Information

ABSTRACT: In this work, we in situ monitor the laser annealing of template-fabricated silver substrates using surface-enhanced Raman scattering (SERS) and 4-mercaptobenzoic acid (4-MBA) as a molecular probe. The annealing process, which exhibits a strong dependence on the laser power, yields a large (>50×) increase in the SERS of the immobilized 4-MBA. This increased SERS response is correlated with the changing substrate morphology using optical and scanning electron microscope images. We attribute the large enhancement to the formation of nanogaps facilitated by binding of the 4-MBA through both thiol and COO groups in a sandwich structure, resulting in both electromagnetic and chemical enhancement. This annealing effect, associated with the continuous increase of SERS intensity, was not limited to the AgNP arrays but included Ag films deposited on a variety of nanoporous templates. This study provides a simple strategy for in situ optimization of plasmonic SERS substrates.



# **■ INTRODUCTION**

Plasmonic effects are extensively applied to manipulate matter at the molecular level and to in situ observe chemical and physical properties upon external stimulus.<sup>1-3</sup> For example, localized surface plasmon resonance (LSPR) biosensors, 4-8 surface-enhanced Raman spectroscopy (SERS), 9-13 optical switches or waveguides, 14,15 and plasmon-enhanced solar cells, 16,17 rely on the properties of the underlying plasmonic substrates. The materials for high-performance plasmonic probes now extend from traditional metals and metallic alloys to semiconductors and carbon-based materials. 18-20 In many cases, the plasmonic substrates can be optimized to produce higher sensitivity by modulating the fabrication procedure to control the size, shape, composition, and pattern of nano-particle arrays. <sup>21–24</sup> Therefore, the ability to fabricate nanostructures with high-resolution and precisely controlled patterns is a major driving force behind the application of plasmonic materials.<sup>25–27</sup>

Thermal annealing $^{28-30}$  and laser-induced annealing $^{31,32}$ provide simple but powerful strategies for improving the performance of plasmonic nanostructures. The thermal approach usually requires high temperature and long annealing times to cause structural alteration in most metallic substrates, whereas the laser approach is more favorable for the localization and patterning of substrates, allowing fine tuning of the plasmonic nanostructures. The annealing effects on plasmonic substrates are commonly characterized by the change of substrate morphology, the shift of LSPR, and the intensity of SERS. The sensitivity of both LSPR and SERS techniques depends strongly on the plasmonic surface of the substrates and their interactions with the excitation light.<sup>33–35</sup> The annealing processes, for example, have been employed to create nanoparticle arrays from metallic films with controllable particle size and density. 36-41 Additionally, annealing can significantly change the morphology, resulting in an LSPR shift and an increased SERS sensitivity. 42,43 Although these measurements provide some information about the annealing process, it would be advantageous to have a direct observation of the sensing performance during the annealing process. In the ideal case, the interaction between the substrate and analyte would be monitored in real time via changes in the spectroscopic signature of the probe. Furthermore, these in situ measurements would provide insight into the detailed mechanism as a function of the laser exposure. In previous work, 44 we found that the symmetric stretch of the carboxylate bands  $(\nu_s(COO^-))$  of 4-mercaptobenzoic acid (4-MBA) is quite sensitive to changes in the interaction between the silver (Ag) surface and the carboxylate group of 4-MBA. This interaction is associated with a shift in the carboxylate frequency from ~1410 cm<sup>-1</sup> for the unbound species to  $\sim$ 1380 or 1360 cm<sup>-1</sup> when the free carboxylate groups become associated with the Ag surface.

In this work, we study laser annealing on several different SERS substrates by monitoring the changing SERS intensity  $(I_{SERS})$  and the Raman band shift of the immobilized 4-MBA as a direct probe of the process. The SERS intensity increases with laser exposure time, and the magnitude depends strongly on the substrate and laser power for all substrates measured here. This increasing SERS intensity is correlated with the changing

Received: February 9, 2018 Revised: April 23, 2018 Published: May 3, 2018

The Journal of Physical Chemistry C

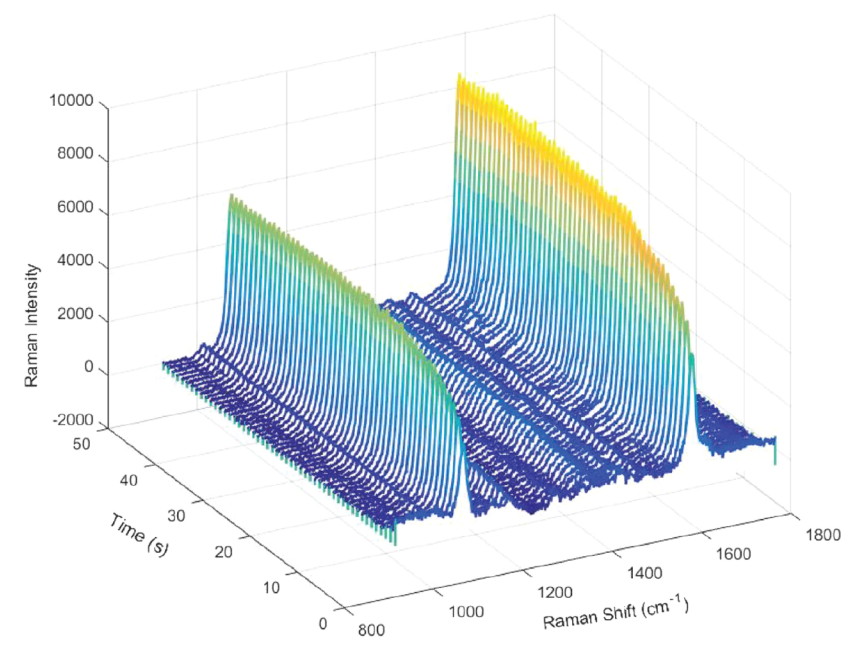


Figure 1. SERS intensity of 4-mercaptobenzoic acid (4-MBA) on AgNP array as a function of time with laser exposure at 500  $\mu$ W (283  $\mu$ W/ $\mu$ m<sup>2</sup>). Raman intensity is given as counts/mW s.

substrate morphology as evidenced by scanning electron microscopy (SEM) studies. Under optimized conditions, more than 50-fold enhancement of 4-MBA SERS was observed. More importantly, we find that the Raman band associated with the symmetric stretch of the carboxylate group ( $\nu_{\rm s}({\rm COO^-})$ ) can serve as a proxy to probe the molecule—substrate interaction. When comparing with the unchanged ring breathing modes of 4-MBA at 1588 cm<sup>-1</sup>, an obvious band shift of  $\nu_{\rm s}({\rm COO^-})$  from ~1410 to 1360 cm<sup>-1</sup> is observed after the laser annealing. This shift indicates an increased interaction between the carboxylate group and silver surface (COO–Ag) during annealing, which is most likely due to the shrinkage of the gap between the nanoscale features.

# EXPERIMENTAL SECTION

Chemical and Materials. All reagents and materials were obtained from Sigma-Aldrich and used as received without further purification. These include 4-mercaptobenzoic acid, 4-hydroxythiophenol (HTP), 1-dodecanethiol (DDT), sodium hydroxide (NaOH), silver nitrite (AgNO<sub>3</sub>), sodium borohydride (NaBH<sub>4</sub>), acetone, hexane, methanol, and chloroform. Glass slides were obtained from VWR, and plain polystyrene nanospheres (600 nm, 10 wt %) from Sigma-Aldrich were diluted 1:1 by methanol prior to use. Chromium (Cr) chips (99.99%) and silver rods (99.999) from Alfa Aesar were used as the metal sources for thermal evaporation. Nanoporous templates used for substrate fabrication include Whatman anodic aluminum membrane (AAO, 0.1 and 0.2  $\mu$ m), osmosis track-etched polycarbonate membrane (TrEM, 0.2  $\mu$ m), and nitrocellulose membrane (NC, 0.22  $\mu$ m).

**Substrate Fabrication.** Silver nanoparticle (AgNP) array substrates were prepared using a procedure similar to the method reported by Martin et al. <sup>45</sup> Briefly, NaBH<sub>4</sub> was dissolved in 50 mM NaOH aqueous solution to give 50 mM NaBH<sub>4</sub>. Then, 50  $\mu$ L of 50 mM AgNO<sub>3</sub> and 250  $\mu$ L of NaBH4/NaOH were added to 5 mL of distilled water (4 °C) with vigorous mixing (vortex mixer) for 30 s. Thereafter, 5 mL of acetone, 5 mL of hexane, and 5  $\mu$ L of DDT were added to

the as-prepared AgNPs aqueous solution. Then, the mixture was vigorously shaken by hand to accelerate the transfer of AgNPs from aqueous phase to hexane phase. The surfactant DDT attaches to the AgNPs surface through the metal-thiol interaction and facilitates transfer of the AgNPs from the densely packed AgNP arrays at the liquid-liquid interface. Immediately, the floating AgNPs arrays were transferred to a precleaned glass slide and then the whole substrate was dried inside the fume hood. Gold nanoparticle (AuNP) array substrates were prepared according to this method by replacing the AgNO<sub>3</sub> stock solution with HAuCl<sub>4</sub> stock solution. Silver nanoporous films (AgNF) were fabricated by thermal deposition of 300 nm Ag film (308R, Ted Pella) on the abovementioned membrane-based templates, including AAO, TrEM, and NC. These templates were then removed by dissolving in 0.1 M NaOH, chloroform, and methanol. The Ag film on nanosphere (AgFON) substrate was prepared by evaporating a 300 nm Ag film on a monolayer of polystyrene nanospheres (600 nm) assembled by following previously established procedures. 46 The PS nanospheres of the AgFON substrates were removed by chloroform to produce Ag pyramid particle arrays (PPA).

**SERS Measurements.** All substrates were immersed in 10 mM 4-MBA or 4-HTP solution for at least 2 h prior to the annealing measurement. To avoid interference from 4-MBA molecules not bound to the surface, we thoroughly rinsed the substrates with methanol after incubation. SERS measurements were conducted on a home-built Raman spectrometer employing a HeNe laser (633 nm, Thorlabs) under ambient condition. The laser beam was focused onto the substrate at 5, 50, 500, or 2000  $\mu$ W using an inverted microscope objective (Nikon, 20×, NA = 0.5). The scattered light was collected by the same objective and after passing through a Rayleigh rejection filter (Semrock) was dispersed in a spectrometer (PI Acton Research, f = 0.3 m, grating = 1200 g/mm). The light is then detected with a back-illuminated deep-depletion CCD (PIXIS, Spec-10, Princeton Instruments). The WinSpec 32 software (Princeton Instruments) was used to operate the spectrometer The Journal of Physical Chemistry C

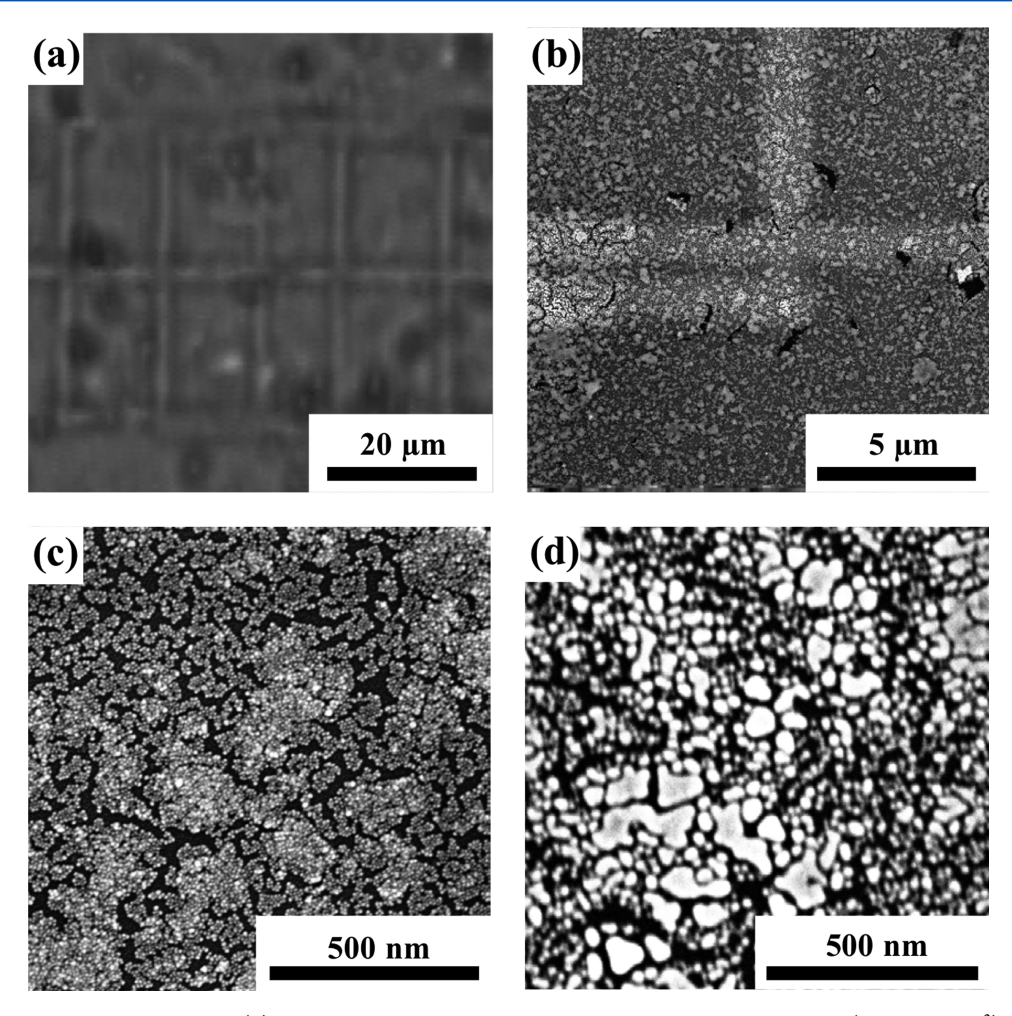


Figure 2. (a) Optical microscopy image and (b) SEM image of the AuNP array after laser exposure at 2000  $\mu$ W (1132  $\mu$ W/ $\mu$ m<sup>2</sup>) for 10 s, illustrating the laser trajectory during annealing. (c, d) The magnified SEM images of unexposed and exposed (annealed) regions, respectively. The small size of nanoparticles shown in (c) becomes much larger in (d) after laser irradiation.

and CCD camera. Integration of 1 s was used for all SERS measurements.

**Morphology Characterization.** A scanning electron microscope (Magellan 400, FEI) was used to collect SEM images of plasmonic substrates before and after laser annealing. After all SERS measurements, 2 nm iridium was sputtered on the substrates to improve the sample conductivity and avoid surface charging during SEM imaging.

## ■ RESULTS AND DISCUSSION

Effect of Laser Power on Annealing. Previous annealing studies of SERS substrates investigate the SERS intensity of the adsorbed molecules before and after annealing under different conditions but did not report on changes during the annealing process.  $^{36,40,47}$  In our experiments, the 4-MBA probe molecule was immobilized on the substrates prior to the annealing process, which was then monitored in situ by continuously acquiring the SERS spectra during annealing. Figure 1 displays the SERS of 4-MBA obtained from AgNP arrays as a function of laser illumination time ( $500~\mu\text{W}$ , 633~nm, 1.0~s scan time for each spectrum). The diameter of laser spot for all experiments is roughly  $1.5~\mu\text{m}$ , leading to a relatively low power density of  $\sim 283~\mu\text{W}/\mu\text{m}^2$ .  $I_{\text{SERS}}$  increases steadily with the scan until reaching a plateau around 20 s. When compared to previous studies of laser-induced annealing employing either higher laser

powers or longer annealing times, we observe larger enhancements at small laser powers and short laser exposure times.<sup>46</sup> The increase of  $I_{\rm SERS}$  is consistent with the results of our ex situ measurements, which also indicated the dependence of  $I_{SERS}$  on the annealing conditions. The AuNP arrays display a clear morphology change as observed in both the optical microscopy (Figure 2a) and SEM (Figure 2b). As shown in Figure 2a, the trajectory of laser movement during the annealing process can be monitored even at low magnification in the optical microscope. Since the image contrast is largely dependent on the ability of matter to scatter, absorb, and transmit the visible light, we attribute the additional image contrast of AuNP arrays to the changed absorption and scattering properties of gold in the range of visible light.<sup>48</sup> Figure 2c,d displays SEM images of the AuNP array substrate before and after laser exposure, respectively. As expected, the morphology of the AuNP arrays changes after laser annealing process. When compared to the relatively small nanoparticle size before annealing, a large nanoparticle size emerges after 10 s of laser irradiation and it is clear that the AuNPs reorganize during annealing.

Furthermore, we investigated the dependence of the annealing on laser power and exposure time by in situ experiments, which monitor the relative intensities and band positions of the carboxylate stretching modes. As shown in Figure 3,  $I_{\rm SERS}$  does not increase appreciably as a function of

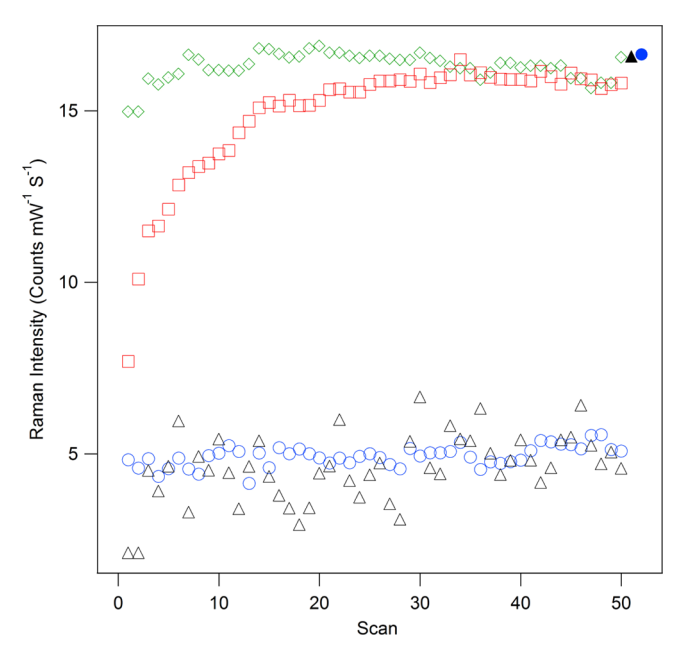


**Figure 3.** Variation of the 4-MBA SERS on AgNP array as a function of laser exposure time for powers of 5  $\mu$ W (black), 50  $\mu$ W (blue), 500  $\mu$ W (red), and 2000  $\mu$ W (green). Solid black triangle and solid blue circle report on the SERS intensity measured using low (5 and 50  $\mu$ W) power after annealing at higher (2000  $\mu$ W) powers, indicating the changes induced are irreversible.

time when the laser power is below 50  $\mu$ W ( $\sim$ 28  $\mu$ W/ $\mu$ m<sup>2</sup>), whereas it increases dramatically for laser powers over 500  $\mu$ W and above. These results indicate a power threshold is required to induce the annealing process, which involves the melting and reconstruction of the nanoparticles. Using higher laser power does not further increase the SERS intensity, and at laser power over 2000  $\mu$ W (1132  $\mu$ W/ $\mu$ m<sup>2</sup>), the SERS signal actually decreases. This decrease might result from damage of probe molecules at high power or elimination of the nanogap features. Figure 4a illustrates high laser influence leads to larger particle size and enlarged interparticle distance. Additionally, the desorption or damage of the 4-MBA molecules could also occur, as suggested by the changing Raman spectrum (Figure 4b). It should also be noted that the increasing SERS signal

arises from an irreversible change of the substrate, since  $I_{\rm SERS}$  measured at low power (5 and 50  $\mu$ W) increases after the annealing when compared to the SERS from the same incident powers before annealing (solid markers, Figure 3). We also consider the dependence of the plasmon resonance spectra on the SERS intensities of the substrate. Our results indicate that SPR spectrum of the exposed region of the annealed substrate can be either blue-shifted or red-shifted when compared with an unexposed region. We believe it is likely due to the breaking down of strong coupling systems, which is consistent with the previous results reported by Itoh and Yamamoto.  $^{49,50}$ 

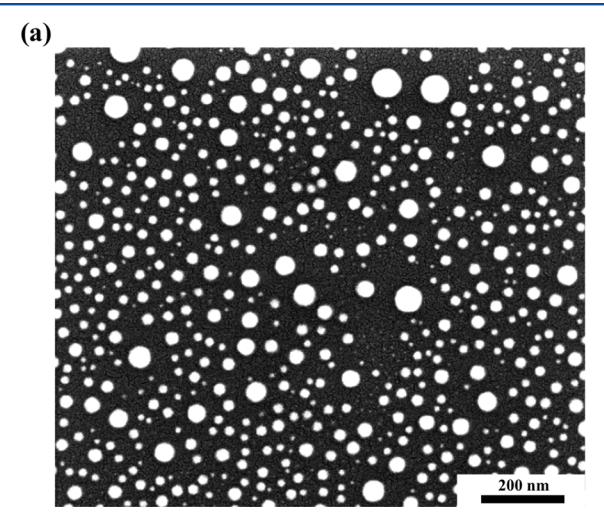
**Substrate Dependence of Annealing.** To further understand the annealing effect, similar measurements were conducted on several other substrates. SEM images of these substrates can be found in Figure S1 of Supporting Information. We test the change of Raman intensity before and after laser exposure of Ag-based substrates prepared by different nanoporous templates. Table 1 summarizes the results

Table 1. Substrate Dependence of Annealing Effect<sup>a</sup>

substrates (metal film-template)	pore/particle size (nm)	$I_{\rm a}/I_{\rm 0}$
AgNP array	20	8
AuNP array	20	7
Ag-AAO	100	57
Ag-AAO	200	23
Ag-NC	220	3
Ag-TrEM	200	1.3
AgFON	600	3
Ag-PPA	600	1.5

 $^aI_0$  and  $I_{\rm a}$  are SERS intensities of 4-MBA before and after annealing at optimized laser power, respectively.

obtained after determining the optimized laser power for each substrate. It can be seen that the increase of SERS intensity due to annealing effect can be generally observed for these substrates, although the magnitude of the increment varies significantly. Figure S2 shows a waterfall plot for the largest increase (57×) observed on Ag nanoporous film (AgNF) fabricated using AAO membrane (100 nm pore size) as template. The large substrate dependence of the annealing is not completely clear. A possible reason is that the annealing



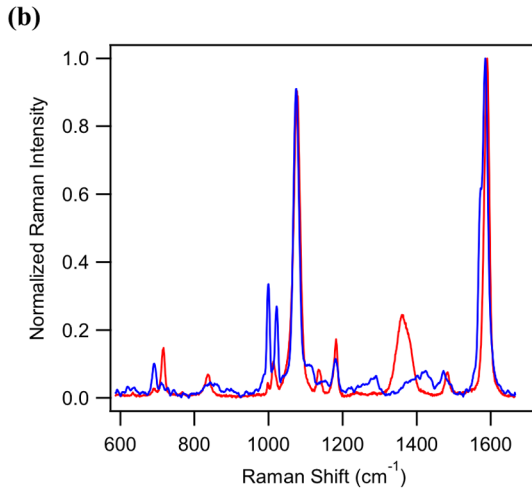


Figure 4. Effect of high laser power on annealing of the SERS substrates and the resulting SERS spectrum. (a) SEM image of AuNP array annealed at 7 mW. (b) Representative SERS spectra of 4-MBA obtained at optimized laser power (red) and overannealed power (blue).

The Journal of Physical Chemistry C

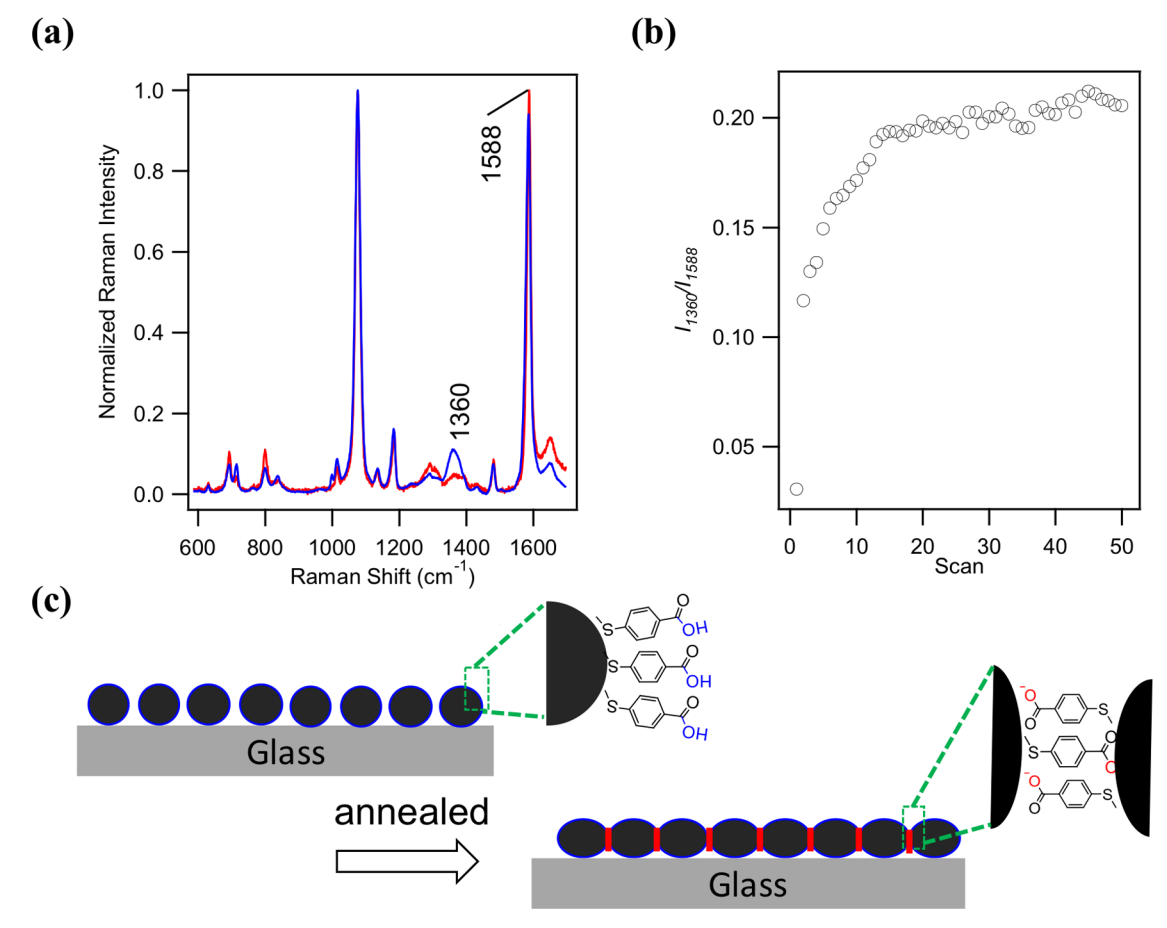


Figure 5. Schematic of the annealing effect showing the increased COO-Ag interaction. (a) SERS spectrum of 4-MBA before (red) and after annealed (blue). (b) The ratio of the Raman intensity of the symmetric stretch carboxylate band  $(I_{1360})$  to the ring breathing mode  $(I_{1588})$  as a function of laser exposure time and (c) proposed mechanism of the annealing effect on COO-Ag interaction.

involves the melting and reconstruction of nanoscale features that lead to the closing of the gap and generation of hot spots that are essential to SERS enhancement, which is less likely to occur on the substrates with much larger gaps. Consequently, substrates with higher density of nanoscale features are more likely to exhibit larger increase of SERS intensity due to annealing. Another explanation is that different substrates may have different heating efficiencies under the same laser condition. This is supported by the fact that the smallest increase was seen on pyramid particle arrays (PPA) and Ag films on track-etched membrane (TrEM), both of which have very low density of nanoscale features. Although most of the substrates are on AgNP and Ag films on templates, a similar annealing effect can be observed on Au nanoparticle (AuNP) arrays. A higher optimized laser power (2000  $\mu$ W) required for observing optimized annealing effect compared with AgNP is likely due to the higher melting temperature of the Au particles.

**Proposed Mechanism of Annealing.** Previous studies suggested that the increase of SERS enhancement results largely from the change of morphology of the substrates upon annealing. <sup>30,51</sup> Figure 2 shows a representative SEM image of the AuNP arrays annealed at optimized laser power. It can be obviously seen that the annealing involves the melting and reconstruction of the metallic features. More importantly, the changing Raman spectrum in Figure 4 plays a key role to explain the mechanism behind the laser annealing process. The annealing process can decrease the gaps between metallic nanoparticles and produce more confined hot spots, which is

reflected by the change of molecular interaction between the probe molecule and substrate surface. This mechanism is supported by the evolution of 4-MBA spectra in the annealing process. In this study, 4-MBA is an ideal probe molecule because it reports on the changing Raman intensity and several of the vibrational bands shift according to their local chemical environment. All 4-MBA bands increase when annealing at the optimized laser power, and the 1360 cm<sup>-1</sup> band additionally exhibits a larger increase (Figure 5a) relative to the other bands. The peak at 1360 cm<sup>-1</sup> is attributed to the symmetric stretch of the  $-COO^-$  interacting with the Ag surface,  $\nu(COO-Ag)$ . As shown in Figure 5b, the additional increase of  $\nu(COO-Ag)$ compared with other modes suggests an increase in the COO-Ag interaction as the gap of AgNPs shrinks. The smaller distances allow the 4-MBA molecules to bridge the gaps in a sandwich geometry through both thiol and carboxylate groups (Figure 5c). The intermediate of bound COO–Ag interaction and unbound COO- interaction further supports this viewpoint (Figure S3). Similar measurements on AgNP arrays and Ag-AAO using 4-hydroxythiophenol (HTP) as a probing molecule produce  $\sim$ 9- and 5-fold increases of  $I_{\rm SERS}$  upon laser annealing. These results support the contribution of the COO-Ag interaction to the SERS enhancement. Overall, although the AgNP and AuNP arrays without annealing exhibit good SERS enhancement, the particle distance of these substrates may not be optimized for SERS measurement. Our proposed laser annealing process can further decrease the gap of the metallic nanoparticles, thus enhancing the interaction between the

probe molecule and substrate surface and then leading to higher signal enhancement.

## CONCLUSIONS

We report the in situ observation of the laser-induced annealing of various plasmonic substrates using SERS measurements. The annealing effect generally increases the SERS intensity and can be observed on many substrates. A strong dependence on laser power is also observed. The change of the SERS intensity is related to the morphology change of the substrates upon annealing, determined by optical and SEM images of the substrates, and increased interaction between the probe molecule and the substrate. The vibrational band  $\nu(\text{COO-Ag})$  also reports on the interaction of the COO— of the 4-MBA molecules and suggests annealing can result in the formation of nanogaps bridged by 4-ABT molecules.

### ASSOCIATED CONTENT

# **S** Supporting Information

The Supporting Information is available free of charge on the ACS Publications website at DOI: 10.1021/acs.jpcc.8b01443.

SEM images of different SERS substrates, Raman spectra of Ag nanoporous film during laser annealing process, and Raman spectrum of the intermediate of bound (Ag—COO) interaction and unbound (COO—) (PDF) In situ laser annealing process on AuNP arrays (AVI)

# AUTHOR INFORMATION

## **Corresponding Author**

\*E-mail: jon.camden@nd.edu.

ORCID ®

Kaiyu Fu: 0000-0002-7899-0388 Paul W. Bohn: 0000-0001-9052-0349 Jon P. Camden: 0000-0002-6179-2692

### **Author Contributions**

§C.M. and K.F. contributed equally to this work.

#### **Notes**

The authors declare no competing financial interest.

# ACKNOWLEDGMENTS

This work was supported by the University of Notre Dame and the U.S. National Science Foundation under CHE-1709566 (C.M., J.P.C.), CHE-1709881 (X.G., M.J.T., J.P.C.), and CHE-1404744 (K.F., P.W.B.), and the National Institute of Allergies and Infectious Diseases under grant 1R01AI113219 (N.B., P.W.B.). Structural characterization of the substrates was performed using the Notre Dame Integrated Imaging Facility whose generous support is gratefully acknowledged.

# REFERENCES

- (1) Zhao, J.; Zhang, C.; Braun, P. V.; Giessen, H. Large-area low-cost plasmonic nanostructures in the NIR for Fano resonant sensing. *Adv. Mater.* **2012**, *24*, OP247—OP252.
- (2) Ciracì, C.; Hill, R. T.; Mock, J. J.; Urzhumov, Y.; Fernandez-Dominguez, A. I.; Maier, S. A.; Pendry, J. B.; Chilkoti, A.; Smith, D. R. Probing the ultimate limits of plasmonic enhancement. *Science* **2012**, 337, 1072–1074.
- (3) Gu, X.; Wang, H.; Camden, J. P. Utilizing light-triggered plasmon-driven catalysis reactions as a template for molecular delivery and release. *Chem. Sci.* **2017**, *8*, 5902–5908.

- (4) Anker, J. N.; Hall, W. P.; Lyandres, O.; Shah, N. C.; Zhao, J.; Van Duyne, R. P. Biosensing with plasmonic nanosensors. *Nat. Mater.* **2008**, *7*, 442–453.
- (5) Brolo, A. G. Plasmonics for future biosensors. *Nat. Photonics* **2012**, *6*, 709–713.
- (6) Willets, K. A.; Van Duyne, R. P. Localized surface plasmon resonance spectroscopy and sensing. *Annu. Rev. Phys. Chem.* **2007**, *58*, 267–297.
- (7) Sepúlveda, B.; Angelome, P. C.; Lechuga, L. M.; Liz-Marzan, L. M. LSPR-based nanobiosensors. *Nano Today* **2009**, *4*, 244–251.
- (8) Mayer, K. M.; Hafner, J. H. Localized surface plasmon resonance sensors. *Chem. Rev.* **2011**, *111*, 3828–3857.
- (9) Stiles, P. L.; Dieringer, J. A.; Shah, N. C.; Van Duyne, R. P. Surface-enhanced Raman spectroscopy. *Annu. Rev. Anal. Chem.* **2008**, 1, 601–626.
- (10) Haes, A. J.; Haynes, C. L.; McFarland, A. D.; Schatz, G. C.; Van Duyne, R. P.; Zou, S. Plasmonic materials for Surface-enhanced sensing and spectroscopy. *MRS Bull.* **2005**, *30*, 368–375.
- (11) Ma, C.; Harris, J. M. Surface-enhanced Raman spectroscopy investigation of the potential-dependent acid—base chemistry of silver-immobilized 2-mercaptobenzoic acid. *Langmuir* **2011**, *27*, 3527–3533.
- (12) Ma, C.; Harris, J. M. Surface-enhanced Raman scattering study of the kinetics of self-assembly of carboxylate-terminated n-alkanethiols on silver. *Langmuir* **2012**, *28*, 2628–2636.
- (13) Schlücker, S. Surface-enhanced Raman spectroscopy: Concepts and chemical applications. *Angew. Chem., Int. Ed. Engl.* **2014**, 53, 4756–4795.
- (14) Maier, S. A.; Brongersma, M. L.; Kik, P. G.; Meltzer, S.; Requicha, A. A. G.; Atwater, H. A. Plasmonics-a route to nanoscale optical devices. *Adv. Mater.* **2001**, *13*, 1501–1505.
- (15) Hsiao, V. K. S.; Zheng, Y. B.; Juluri, B. K.; Huang, T. J. Light-driven plasmonic switches based on Au nanodisk arrays and photoresponsive liquid Crystals. *Adv. Mater.* **2008**, *20*, 3528–3532.
- (16) Nakayama, K.; Tanabe, K.; Atwater, H. A. Plasmonic nanoparticle enhanced light absorption in GaAs solar cells. *Appl. Phys. Lett.* **2008**, *93*, No. 121904.
- (17) Atwater, H. A.; Polman, A. Plasmonics for improved photovoltaic devices. *Nat. Mater.* **2010**, *9*, 205–213.
- (18) West, P. R.; Ishii, S.; Naik, G. V.; Emani, N. K.; Shalaev, V. M.; Boltasseva, A. Searching for better plasmonic materials. *Laser Photonics Rev.* **2010**, *4*, 795–808.
- (19) Naik, G. V.; Shalaev, V. M.; Boltasseva, A. Alternative plasmonic materials: Beyond gold and silver. *Adv. Mater.* **2013**, *25*, 3264–3294.
- (20) Boriskina, S. V.; Ghasemi, H.; Chen, G. Plasmonic materials for energy: From physics to applications. *Mater. Today* **2013**, *16*, 375–386.
- (21) Srituravanich, W.; Fang, N.; Sun, C.; Luo, Q.; Zhang, X. Plasmonic nanolithography. *Nano Lett.* **2004**, *4*, 1085–1088.
- (22) Sönnichsen, C.; Reinhard, B. M.; Liphardt, J.; Alivisatos, A. P. A molecular ruler based on plasmon coupling of single gold and silver nanoparticles. *Nat. Biotechnol.* **2005**, 23, 741–745.
- (23) Ding, B.; Deng, Z.; Yan, H.; Cabrini, S.; Zuckermann, R. N.; Bokor, J. Gold nanoparticle self-similar chain structure organized by DNA origami. *J. Am. Chem. Soc.* **2010**, *132*, 3248–3249.
- (24) Gao, B.; Arya, G.; Tao, A. R. Self-orienting nanocubes for the assembly of plasmonic nanojunctions. *Nat. Nanotechnol.* **2012**, *7*, 433–427
- (25) Tripp, R. A.; Dluhy, R. A.; Zhao, Y. Novel nanostructures for SERS biosensing. *Nano Today* **2008**, *3*, 31–37.
- (26) Biener, J.; Nyce, G. W.; Hodge, A. M.; Biener, M. M.; Hamza, A. V.; Maier, S. A. Nanoporous plasmonic metamaterials. *Adv. Mater.* **2008**, *20*, 1211–1217.
- (27) Jahn, M.; Patze, S.; Hidi, I. J.; Knipper, R.; Radu, A. I.; Muhlig, A.; Yuksel, S.; Peksa, V.; Weber, K.; Mayerhofer, T.; et al. Plasmonic nanostructures for surface enhanced spectroscopic methods. *Analyst* **2016**, *141*, 756–793.
- (28) Zhang, X.; Liu, H.; Pang, Z. Annealing process in the refurbishment of the plasmonic photonic structures fabricated using colloidal gold nanoparticles. *Plasmonics* **2011**, *6*, 273–279.

- (29) Jia, K.; Bijeon, J.-L.; Adam, P.-M.; Ionescu, R. E. Large scale fabrication of gold nano-structured substrates via high temperature annealing and their direct use for the LSPR detection of atrazine. *Plasmonics* **2013**, *8*, 143–151.
- (30) Zhou, J.; Liu, H.; Wang, T.; Li, Y.; Zhang, J.; Lu, Z.; Fu, Y.; Li, F. Adjusting the inter-particle spacing of a nanoparticle array at the subnanometre scale by thermal annealing. *Chem. Commun.* **2014**, *50*, 14547–14549.
- (31) Henley, S. J.; Beliatis, M. J.; Stolojan, V.; Silva, S. R. Laser implantation of plasmonic nanostructures into glass. *Nanoscale* **2013**, 5, 1054–1059.
- (32) Arnob, M. M.; Zhao, F.; Zeng, J.; Santos, G. M.; Li, M.; Shih, W. C. Laser rapid thermal annealing enables tunable plasmonics in nanoporous gold nanoparticles. *Nanoscale* **2014**, *6*, 12470–12475.
- (33) Wang, H.; Levin, C. S.; Halas, N. J. Nanosphere arrays with controlled sub-10-nm gaps as surface-enhanced Raman spectroscopy substrates. *J. Am. Chem. Soc.* **2005**, *127*, 14992–14993.
- (34) Wustholz, K. L.; Henry, A.-I.; McMahon, J. M.; Freeman, R. G.; Valley, N.; Piotti, M. E.; Natan, M. J.; Schatz, G. C.; Van Duyne, R. P. Structure-activity relationships in gold nanoparticle dimers and trimers for Surface-enhanced Raman spectroscopy. *J. Am. Chem. Soc.* **2010**, *132*, 10903–10910.
- (35) Park, W.-H.; Kim, Z. H. Charge transfer enhancement in the SERS of a single molecule. *Nano Lett.* **2010**, *10*, 4040–4048.
- (36) Kwon, C. H.; Boo, D. W.; Hwang, H. J.; Kim, M. S. Temperature dependence and annealing effects in surface-enhanced Raman scattering on chemically prepared silver island films. *J. Phys. Chem. B* **1999**, *103*, 9610–9615.
- (37) Lu, Y.; Liu, G. L.; Lee, L. P. High-density silver nanoparticle film with temperature-controllable interparticle spacing for a tunable surface enhanced Raman scattering substrate. *Nano Lett.* **2005**, *5*, 5–9.
- (38) Hu, A.; Peng, P.; Alarifi, H.; Zhang, X. Y.; Guo, J. Y.; Zhou, Y.; Duley, W. W. Femtosecond laser welded nanostructures and plasmonic devices. *J. Laser Appl.* **2012**, *24*, No. 042001.
- (39) Lee, S.; Hahm, M. G.; Vajtai, R.; Hashim, D. P.; Thurakitseree, T.; Chipara, A. C.; Ajayan, P. M.; Hafner, J. H. Utilizing 3D SERS active volumes in aligned carbon nanotube scaffold substrates. *Adv. Mater.* **2012**, *24*, 5261–5266.
- (40) Xu, W.; Xiao, J.; Chen, Y.; Chen, Y.; Ling, X.; Zhang, J. Graphene-veiled gold substrate for surface-enhanced Raman spectroscopy. *Adv. Mater.* **2013**, 25, 928–933.
- (41) Liu, H.; Zhang, X.; Zhai, T.; Sander, T.; Chen, L.; Klar, P. J. Centimeter-scale-homogeneous SERS substrates with seven-order global enhancement through thermally controlled plasmonic nanostructures. *Nanoscale* **2014**, *6*, 5099–5105.
- (42) Fujimaki, M.; Awazu, K.; Tominaga, J.; Iwanabe, Y. Surface-enhanced Raman scattering from Ag nanoparticles formed by visible laser irradiation of thermally annealed AgOx thin films. *J. Appl. Phys.* **2006**, *100*, No. 074303.
- (43) Kucheyev, S. O.; Hayes, J. R.; Biener, J.; Huser, T.; Talley, C. E.; Hamza, A. V. Surface-enhanced Raman scattering on nanoporous Au. *Appl. Phys. Lett.* **2006**, *89*, No. 053102.
- (44) Ma, C.; Trujillo, M. J.; Camden, J. P. Nanoporous silver film fabricated by oxygen plasma: A facile approach for SERS substrates. ACS Appl. Mater. Interfaces 2016, 8, 23978–23984.
- (45) Martin, M. N.; Basham, J. I.; Chando, P.; Eah, S.-K. Charged gold nanoparticles in non-polar solvents: 10-min synthesis and 2D self-assembly. *Langmuir* **2010**, *26*, 7410–7417.
- (46) Fu, K.; Han, D.; Ma, C.; Bohn, P. W. Electrochemistry at single molecule occupancy in nanopore-confined recessed ring-disk electrode arrays. *Faraday Discuss.* **2016**, *193*, 51–64.
- (47) Viets, C.; Hill, W. Laser power effects in SERS spectroscopy at thin metal films. *J. Phys. Chem. B* **2001**, *105*, 6330–6336.
- (48) Jain, P. K.; Lee, K. S.; El-Sayed, I. H.; El-Sayed, M. A. Calculated absorption and scattering properties of gold nanoparticles of different size, shape, and composition: Applications in biological imaging and biomedicine. *J. Phys. Chem. B* **2006**, *110*, 7238–7248.
- (49) Itoh, T.; Yamamoto, Y. S.; Tamaru, H.; Biju, V.; Wakida, S.-I.; Ozaki, Y. Single-molecular surface-enhanced resonance Raman

- scattering as a quantitative probe of local electromagnetic field: The case of strong coupling between plasmonic and excitonic resonance. *Phys. Rev. B* **2014**, *89*, No. 195436.
- (50) Yamamoto, Y.S.; Itoh, T. Why and how do the shapes of surface-enhanced Raman scattering spectra change? Recent progress from mechanistic studies. *J. Raman Spectrosc.* **2016**, *47*, 78–88.
- (51) Imamova, S.; Nedyalkov, N.; Dikovska, A.; Atanasov, P.; Sawczak, M.; Jendrzejewski, R.; Śliwiński, G.; Obara, M. Near field properties of nanoparticle arrays fabricated by laser annealing of thin Au and Ag films. *Appl. Surf. Sci.* **2010**, *257*, 1075–1079.